Title
Effective Stress in Unsaturated Silt at Low Degrees of Saturation

Journal
Vadose Zone Journal, 13(5)

ISSN
1539-1663

Authors
Alsherif, NA
McCartney, JS

Publication Date
2014-05-01

DOI
10.2136/vzj2013.06.0109

Peer reviewed

Effective Stress in Unsaturated Silt at Low Degrees of Saturation

N.A. Alsherif and J.S. McCartney*

N.A. Alsherif and J.S. McCartney
Department of Civil, Environmental, and Architectural Engineering
University of Colorado Boulder, UCB 428, Boulder, CO 80309.
*Corresponding author (john.mccartney@colorado.edu)

Abstract

This paper presents an evaluation of the effective stress concept in unsaturated, compacted silt at low degrees of saturation. A set of isothermal, consolidated-drained triaxial tests was performed on silt specimens under different combinations of total suction and net normal stress. The total suction was controlled using an automated humidity system, and variables monitored during equilibration and shearing include isotropic volume change, axial displacement, temperature, relative humidity at the top and bottom of the specimen, and the gas pressure difference across the specimen. The results from the triaxial tests were analyzed to examine the applicability of predicting the suction-stress characteristic curve (SSCC) using parameters from soil-water retention curve (SWRC) models fitted to experimental data obtained at low suction magnitudes. The SSCC predicted from the SWRC at low suctions was found to over-predict the suction stress values at high suctions obtained from back-extrapolation of the failure envelope to define the tensile strength. However, small adjustments in the fitting of the SWRC were found to provide a better fit between the SSCC and experimental suction stress data. The suction stress defined using the adjusted SWRC was found to provide a good interpretation of the critical state line in terms of mean effective stress over both high and low suction ranges.

Keywords: SWRC; suction stress; unsaturated soils; effective stress

Introduction

Many of the previous studies on the principle of effective stress in unsaturated soils used the axis translation technique to characterize the shear strength or volume change of soil specimens having relatively high degrees of saturation (Khalili et al. 2004; Lu and Likos 2006; Khalili and Zargarbashi 2010; Alonso and Romero 2011). At these relatively high degrees of saturation, typically greater than 0.5, the water phase is likely connected through the specimen. Khalili and Khabbaz (1998), Lu and Likos (2006), Kayadelen et al. (2007), and Lu et al. (2010) have shown experimentally and analytically that the soil-water retention curve (SWRC) and the effective stress are functionally related, and these relationships are assumed to hold over the whole range of saturation. Lu et al. (2010) proved that the van Genuchten (1980) SWRC model can be used to define the effective stress in both unsaturated sands and clays, and found analytically that the effective stress for clays should monotonically increase with increasing suction for the case of constant net normal stress.

Despite the strong evidence supporting a relationship between the SWRC and effective stress, this relationship has not been fully verified at high suction magnitudes (or low degrees of saturation) where the water phase is not continuous. This is a critical gap in the literature because it is common practice to extrapolate the shape of the SWRC fitted to data at high degrees of saturation to the entire range of degree of saturation. Even when SWRC data is defined at high suctions using separate tests, the uncertainty in the data may be particularly high due to specimen variability, changes in volume, large changes in suction with relatively small changes in relative humidity of the pore air, and issues with defining thermodynamic equilibrium (Blatz et al. 2008; Delage et al. 2008).

The objective of this study is to evaluate the effective stress principle for compacted silt specimens at low degrees of saturation and assess the implications of using a single SWRC curve fitted to data obtained at low suction magnitudes to predict the effective stress state over the full range of saturation. These topics are relevant as it is possible to encounter fundamental changes in the inter-particle stresses in the transitions between the three saturation ranges of the primary drying-path SWRC (Lu and Likos 2004). The first range is the saturated range within which the soil can be considered fully saturated, which extends from zero suction up to the air entry suction. In this range, the negative water pressure can be incorporated directly into Terzaghi's definition of effective stress ($\sigma' = \sigma - u_w$). The second range is the funicular range where air enters the pores of the soil displacing pore water, leading to a significant decrease in the degree of saturation decreases with increasing suction. In the funicular region, the shear strength (Blatz and Graham 2000; Rahardjo et al. 2003; Ajdari et al. 2010) and elastic moduli (Ng et al. 2009; Khosravi and McCartney 2012) of fine-grained soils increase significantly. The third range is the pendular or residual saturation range where the pore water resides as isolated pendular menisci. In this range, van der Waals attraction forces play an important role in the inter-particle stresses in fine grained soils (Lu and Likos 2006), and several studies have found that the shear strength of soils can be significantly greater than that in the funicular range (Blatz et al. 2002; Nishimura and Fredlund 2000). The transition from the funicular to pendular ranges occurs at different degrees of saturation for different soils, and it is typically necessary to use vapor equilibrium techniques to change the water content of the soil beyond this point. The residual saturation S_{res} can be defined as the irreducible saturation at which water is bonded to the soil particles hydroscopically and can only be removed using oven drying (Brooks and Corey 1964).

To accomplish the objective of this study, a new triaxial cell was developed that has the capability of measuring the shear strength of unsaturated soils under high suction magnitudes ranging from 15 to 325 MPa. Specifically, the vapor flow technique developed by Likos and Lu (2003) was employed in the triaxial cell to control the relative humidity within a silt specimen to reach degrees of saturation in the pendular range (i.e., less than 0.11). Consolidated drained (CD) triaxial compression tests were performed to measure the drained shear strength failure envelope of unsaturated silt specimens under high suction magnitudes, with the goal of evaluating the suitability of defining the effective stress using the suction stress characteristic curve (SSCC) approach of Lu and Likos (2006). Further, another goal of this study is to predict the SSCC from the SWRC defined using data from the axis translation technique at low suction magnitudes is also used to provide a predictive assessment of the SSCC and effective stress using relationships defined by Lu et al. (2010). A comparison of the predicted SSCCs using the two different testing techniques permits evaluation of the linkage between the SWRC and SSCC at low degrees of saturation. Ajdari et al. (2010) also investigated the shear strength of compacted bentonite specimens using direct shear tests, and measured the suction using the filter paper method at the end of shearing. Although they observed a clear relationship between the shear strength and effective stress for suctions up to 287 MPa, they did not control suction in their tests and may have only approached the beginning of the residual saturation range for the compacted bentonite in their tests.

Background

Bishop (1959) formulated a relationship for the effective stress in unsaturated soils that incorporated a soil-specific effective stress parameter χ to account for the impact of the amount of pore water, as follows:

$$\sigma' = (\sigma - u_a) + \chi(u_a - u_w) \quad (1)$$

where the difference between the total normal stress σ and the pore air pressure u_a is referred to as the net normal stress σ_n, and the difference between the pore air pressure u_a and the pore water pressure u_w is referred to as the suction ψ, and χ is referred to as the effective stress parameter. Skempton (1961) defined a general equation for the effective stress in unsaturated soils building upon the relationship of Bishop (1959) that considers the relative compressibility values of the soil skeleton and soil particles and the effects of saturation:

$$\sigma' = \sigma - \left(1 - \frac{c_s}{c}\right) S_\chi u_w \quad (2)$$

where σ′ is the effective stress, c_s is the compressibility of the grains, c is the compressibility of the granular skeleton, u_w is the pore water pressure, and S_χ is a scaling parameter for saturation defined using the χ value used in Bishop's (1959) definition of effective stress. Skempton (1961) used this equation to evaluate the need for considering the role of pore water pressure in stiffer materials like rock and concrete. This equation indicates that the definition of a single-value effective stress for both saturated and unsaturated soils requires knowledge of the material properties of the soil.

Difficulties were encountered in selecting an appropriate definition of the effective stress parameter due to issues such as hysteresis and volume change (Blight 1967). In attempting to overcome these issues, while also eliminating the necessity to define the effective stress parameter, Lu and Likos (2006) referred to the second term in Equation 2 as the suction stress σ_s, a material relationship that is a function of suction or the degree of saturation, S_r. Lu and Likos (2006) defined the suction stress σ_s as a macroscopic stress that collectively incorporates the effects of capillarity, soil- and pore fluid-specific forces such as van der Waals forces, electrical

double-layer repulsion forces, and the net attraction forces arising from chemical cementation at the grain contacts. The functional relationship between suction stress and suction for a given soil under a certain stress state was referred to as the suction stress characteristic curve (SSCC).

Lu and Likos (2006) proposed an empirical approach to determine the SSCC using shear strength failure envelopes defined from drained shear strength tests performed on saturated and unsaturated soil specimens under controlled values of matric suction as shown in Figure 1. Although the failure envelopes are plotted as a function of net normal stress in this figure, they still represent effective failure envelopes as they should be defined from drained tests. Lu and Likos (2006) assumed that the suction stress σ_s at a given suction ψ is equal to the apparent tensile strength, which could be calculated from the intercept of the failure envelopes with the normal stress axis as follows:

$$\sigma_s = \frac{c}{\tan(\phi')} \tag{3}$$

where c is the apparent cohesion of the soil due to the effects of suction and ϕ' is the effective friction angle. To define the SSCC shown in the schematic in Figure 1, the apparent cohesion for saturated soils tested under drained conditions is assumed negligible, which is the case for uncemented soils, and the friction angle is assumed to be constant with confining stress. Further, it is assumed that the friction angle does not change when different suction values are applied to the soil (Escario 1980; Nishimura and Fredlund 2000). This assumption may only be valid for the case of rigid soils that do not change in volume during changes in matric suction (*e.g.*, sands, silts, and clays of low plasticity). Changes in σ_s and the effective stress parameter χ with suction have been evaluated for different soils using the approach similar to that shown in Figure 1 (Khalili and Khabbaz 1998; Lu and Likos 2006; Khosravi et al. 2012).

It is a common assumption that the effective stress parameter was related to the degree of saturation in representing the shear strength of soils (Bishop and Donald 1961; Oberg and Sallfors 1997) and in elasto-plastic constitutive relationships (Hassanizadeh and Gray 1990; Houlsby 1997; Gray and Schrefler 2001; Gallipoli et al. 2003; Wheeler et al. 2003; Tamagnini 2004; Nuth and Laloui 2008; Alonso and Romero 2011). This assumption may not work well for some soils, and relatively large discrepancies have been observed in some early studies (Bishop and Blight 1963). Other studies have used the effective saturation [$S_e = (S-S_{res})/(1-S_{res})$] as the effective stress parameter successfully to evaluate the shear strength and elastic modulus of unsaturated soil (Vanapalli et al. 1996; Lu et al. 2010; Khosravi et al. 2011; Khosravi and McCartney 2012). More complicated functions of degree of saturation have also been proposed (Toll and Ong 2003; Sheng et al. 2008), while some studies have shown the utility of empirical relationships. Khalili and Khabbaz (1998) defined the effective stress parameter as a power-law relationship involving the ratio of the suction and the air entry suction, which has been applied in constitutive models (Lloret and Khalili 2002) and in re-examining data from the literature (Khalili et al. 2004). Khalili and Zargarbashi (2010) performed staged triaxial tests on unsaturated soil specimens during wetting, and observed that the effective stress parameter is sensitive to hydraulic hysteresis. Further, they found that the use of an effective stress parameter equal to the degree of saturation may not be suitable for all soils during hydraulic hysteresis. Nonetheless, Khosravi and McCartney (2012) found that the effective stress parameter defined as the effective saturation also permits reasonable assessment of changes in shear modulus during hydraulic hysteresis. It is also possible that application of net stresses may also affect the effective stress parameter, as volume changes may affect the shape of the SWRC especially at low suction magnitudes (Ng and Pang 2000).

A closed-form equation for the suction stress was proposed by Lu et al. (2010) by employing the effective saturation as the effective stress parameter χ. This permits integration of the van Genuchten (1980) SWRC into the definition of the suction stress. The van Genuchten (1980) SWRC model in terms of the degree of saturation S is given as:

$$S = \frac{S_{res} + (1 - S_{res})}{\left(1 + [\alpha_{vG}(u_a - u_w)]^{N_{vG}}\right)^{1-\frac{1}{N_{vG}}}} \tag{4}$$

where S_{res} is the residual degree of saturation, and N_{vG} and α_{vG} are empirical parameters used to fit the SWRC to experimental SWRC data. The parameter α_{vG} is typically considered to be the inverse of air entry suction and the parameter N_{vG} is related to the pore size distribution and describes the slope of the SWRC for suctions between the air entry suction and the residual degree of saturation. The suction stress can be predicted by combining Equation (4) with Equation (1), as follows (Lu et al. 2010):

$$\sigma_s = \frac{(u_a - u_w)}{\left(1 + [\alpha_{vG}(u_a - u_w)]^{N_{vG}}\right)^{\frac{N_{vG}-1}{N_{vG}}}} \qquad u_a - u_w \geq 0 \tag{5}$$

where N_{vG} and α_{vG} are the parameters fitted to experimental SWRC data points. Further, by substituting Equation (5) into Equation (1), the effective stress can be defined for unsaturated soils as follows (Lu et al. 2010):

$$\sigma' = (\sigma - u_a) + \frac{(u_a - u_w)}{\left(1 + [\alpha_{vG}(u_a - u_w)]^{N_{vG}}\right)^{\frac{N_{vG}-1}{N_{vG}}}} \qquad u_a - u_w \geq 0 \tag{6}$$

Lu et al. (2010) validated Equation (6) for both sands and clays using suction stress values obtained from shear strength tests using Equation (3), albeit primarily for low suction magnitudes (up to 1500 kPa) and relatively high degrees of saturation (in the range of 1.00 to 0.35). They found that the predicted SSCC for clay increased monotonically with suction, while

the predicted SSCC for sand increased to a maximum value, then decreased back to zero. Lu et al. (2010) also proved that fine-grained soils like silt and clay should experience a monotonic increase in inter-particle stresses when the van Genuchten (1980) model parameter N_{vG} is greater than 2. Khosravi et al. (2012) and Lu et al. (2013) also observed an increasing trend in suction stress with suction for a sand-silt mixture and a clay, respectively, verifying this prediction for low suctions. However, the suitability of extrapolating the analytical expression for effective stress in Equation (6) to high suction magnitudes has not been evaluated.

Evaluation of the SSCC equation of Lu et al. (2010) indicates that the suction stress at high suction magnitudes is very sensitive to the value of N_{vG}. A parametric analysis of the impact of N_{vG} on the shapes of the SWRC and SSCC for a constant value of α_{vG} = 0.60 kPa^{-1} is shown in Figures 2(a) and 2(b) in terms of the SSCC and SWRC, respectively. The results in these figures indicate that relatively small changes in N_{vG} can have a significant impact on the amount of water stored in the soil as well as the magnitude of suction stress at high suctions. Specifically, larger values of N_{vG} lead to a decrease in the volume of water stored in the soil as well as a lower suction stress. The results in Figure 2(a) indicate that soils with higher N_{vG} values will experience a significantly greater increase in suction stress with suction compared with soils having only slightly smaller values of N_{vG}.

Testing Apparatus

Triaxial cell

A triaxial cell is designed to accommodate the application of high suction magnitudes using an automated humidity system with continuous gas flow as well as elevated temperatures. A drawing of the modified triaxial cell with its different components is shown in Figure 3. Duran

Borosilicate glass tubing having an outer diameter of 180 mm, a wall thickness of 9 mm and a length of 381 mm is used as the pressure vessel for the triaxial cell.

Suction control system

Inside the triaxial cell, the upper and lower parts of the platen are designed to allow the application of high suction using the automated humidity system with continuous gas flow, which allows testing soils under conditions where the flow of air is dominant. The gas flow system consists of a computer-automated humidity-control system developed previously by Likos and Lu (2001) which permits automated control of the relative humidity of the pore air (and consequently control of the total suction applied to the soil specimen) while making sure that the temperature of the gas stream is the same as that within the specimen. The relative humidity in this system is controlled using computer-controlled proportional valves to partition the mixture of vapor-saturated, or 'wet', N_2 gas and desiccated, or 'dry', N_2 gas.

A schematic of the automated humidity-control system is shown in Figure 3. Nitrogen is passed from a pressure regulated bottle through 6.3 mm-diameter perfluoroalkoxy (PFA) tubing, which is split into two separate gas streams through a pair of computer-controlled mass-flow valves (MKS Instruments, Type 1179A). These valves can regulate the flow of each gas stream between zero and 3.3×10^{-6} m^3/s based on a signal from a controlling National Instruments LabView data acquisition program. The first gas stream is vapor-saturated by bubbling it through a bottle filled with distilled water and placed on a thermo scientific heating machine to implement the same target temperature being applied to the soil specimen. The second gas stream is routed through a Hammond cylinder filled with color-indicating drierite desiccant media (calcium sulfate, >98% $CaS0_4$, >2% $CaCl_2$). The two gas streams (wet and dry) are reintroduced later into a mixing chamber at a combined flow rate of 3.3×10^{-6} m^3/s. The combined

gas stream, having a relative humidity that is a direct function of the 'wet' to 'dry' gas flow ratio (w/d), is forced through the bottom and vented from the top of the soil specimen. After reaching steady-state gas flow through the specimen, the relative humidity of the gas can be adjusted using a feedback-control system that monitors the relative humidity and temperature at the bottom of the specimen with a probe (Model HMT330 from Vaisala, Inc.). This probe is connected to the bottom of the soil specimen through the platen allowing for continuous measurement and monitoring during testing. This probe can be pressurized up to 407 kPa. It works properly for all values of relative humidity exposed to temperatures ranging from -70 to +180°C while also maintaining a high resistance to corrosion. A rigid porous disk separates the bottom of the specimen from being in touch with the head of the probe to avoid the issue of any possible influence of the sensor itself on the mechanical performance of the specimen. The probe is connected to a transmitter that transfers the recorded data to the computer program. Signals from the humidity probe work as a feedback loop with the controlling computer program for automated regulation of the 'wet' to 'dry' gas flow ratio (w/d) using the two mass-flow controllers. The top of the specimen is connected to an insulated bottle containing a second relative humidity sensor to monitor the relative humidity of the gas passing from the top of the specimen. This bottle is vented to the atmosphere (i.e., zero air pressure at the top of the specimen). Nitrogen gas at a constant pressure of 262 kPa is pressurized from the Nitrogen bottle through the mass flow control valves to adjust the value of gas pressure applied to the bottom of the soil specimen up to 40 kPa and vented from the top. When the relative humidity values of the inlet and outlet gases are the same, then the specimen is assumed to be in equilibrium with a total suction. This assumption is based on the idea that constant relative humidity is applied to the bottom of soil specimen and the flow of gas one-dimensional from the bottom to the top of

specimen. This means that the decrease in relative humidity progresses upward through the specimen until equilibration occurs. The total suction is predicted using Kelvin's law, as follows:

$$\psi = \frac{\rho_w RT}{M_w} \ln\left(\frac{R_h}{100}\right) \tag{7}$$

where ψ is the total suction (kPa), R is the universal (molar) gas constant, equal to 8.31432 J/molK, T is the absolute temperature in Kelvin, M_W is the molecular mass of water vapor equal to 18.016 g/mol, ρ_w is the density of water (kg/m^3), and R_h is the relative humidity of the pore air in percent. In addition, a differential pressure transducer (DPT) connected to the top and bottom of soil specimen is used to monitor the differential pressure across the specimen. As the pressure at the base was 40 kPa while the pressure was 0 kPa at the top, the average air pressure in the specimen

Mechanical loading system

A Brainard-Kilman Model S-600 triaxial load frame is adapted in this study to apply loads to the triaxial cell in either load-control or displacement-control conditions. In normal operation, this load frame can be used to apply constant displacement rates to shear a soil specimen in displacement-controlled conditions. In addition, a pneumatic piston is incorporated into the top beam of the triaxial cell to apply load-controlled conditions to the specimen. Utilizing a load-controlled procedure allows the soil specimen to deform freely in the axial direction during changes in suction or temperature while maintaining a constant axial load. In either configuration, a load cell is used to record axial loads applied to the specimen during shearing. The axial displacement during all stages of suction application, heating and shearing is also measured using a linearly variable differential transformer (LVDT) connected to the top piston. In this test setup, volume change of the soil specimen due to changes in suction, temperature, or shearing is monitored by recording the change of water level in a graduated burette connected to

the water supply line of the cell pressure using a differential pressure transducer. Calibration tests were performed to quantify the impact of cell pressure and temperature on the volume measurement system (Alsherif and McCartney 2013).

Materials

ML silt obtained from the Bonny Dam on the Colorado-Kansas border was used in this experimental study. A summary of the index properties of Bonny silt is shown in Table 1. The drying-path soil water retention curve (SWRC) for Bonny silt compacted to a void ratio of 0.68 is shown in Figure 4. The flexible-wall permeameter setup developed by McCartney and Znidarcic (2010) was used to measure the points on the SWRC at low suction magnitudes. Their approach combines the axis translation technique for suction control with a flow pump to track changes in degree of saturation of the specimen as water is drawn from the specimen in stages. The change in suction during operation of the pump was monitored using a differential pressure transducer connected to the top of the specimen to measure air pressure and the bottom of the specimen to measure water pressure. An interesting feature of the data points on the SWRC obtained using the flexible-wall permeameter setup is that amount of water extracted from the specimen started to decrease significantly after drying the specimen to a degree of saturation of approximately 0.65. This is not due to double porosity effects, but occurred because the water phase in the silt started to become discontinuous, making it impossible to withdraw further amounts of water from the specimen with the pump. This behavior was also observed by Khosravi and McCartney (2012) for the same soil but under different initial void ratios.

The van Genuchten (1980) SWRC relationship in Equation (4) was fitted to the experimental data between degrees of saturation of 1.0 and 0.67 using least squares minimization, as shown in Figure 4. The parameters α_{vG} and N_{vG} shown in Figure 4 are representative of the SWRC

obtained from data at low suction magnitudes extrapolated to high suction magnitudes. In addition to the low suction data, two data points from high suction magnitudes obtained using the vapor flow technique and corresponding to the conditions investigated in this study are shown in Figure 4. Although the van Genuchten (1980) SWRC was fitted to the low suction data, it appears to provide a good fit to the high suction data as well.

Specimen Setup and Test Procedures

The specimens evaluated in this study were prepared using static compaction. Prior to compaction, the soil was oven-dried at a temperature of 110 °C for 24 h, ground using a rubber hammer, and screened through a No. 40 sieve. It was then carefully wetted with a spray gun to an initial water content of 10.5% and placed in a sealed plastic bag to cure for 24 hours so that the water content could homogenize. A compaction water content of 10.5% corresponds to a water content that is 8% dry of optimum. The reason for selecting such a low compaction water content was to prepare specimens with a low enough initial degree of saturation such that their air permeability would be high enough to permit rapid gas flow through the specimen in the vapor flow technique, leading to faster suction equilibration. The soil, having a specific gravity of 2.65, was compacted using a mechanical press in three lifts having thicknesses of 24 mm in a 35 mm-diameter mold to a dry unit weight of 15.7 kN/m^3 and initial degree of saturation of 0.41. This corresponds to an initial void ratio of 0.68. To avoid the presence of weak zones within the samples, the interfaces between lifts were scarified with a blade. The sample was then weighed and the dimensions were measured using a Vernier caliper.

After preparing a soil specimen, a coarse porous stone and a filter paper having the same diameter as the specimen were placed atop the lower platen of the triaxial cell. The specimen was placed atop this assembly. Another filter paper, coarse porous stone and the top platen were

placed atop the specimen. A 0.635 mm-thick latex membrane was placed around the soil specimen. Two "O"-rings were placed around the latex membranes on the top and bottom platens to provide a reliable seal at low confining stresses. Next, the relative humidity probe and thermocouple were connected to the bottom and top of the cell, respectively. After the glass cell was placed between the top and bottom caps of the triaxial cell, the cell was filled with de-aired water at room temperature and placed on the load frame. An LVDT was mounted to the piston to monitor axial displacements.

The differential pressure transducer used to monitor the air pressure gradient across the specimen was attached to the top and bottom ports to the specimen. The ports for the automated humidity system were connected to the cell. At this stage the water circulation pump was started and the desired confining stress was applied to the triaxial cell. The pump operation was not affected by the increase in pressure within the cell, and the pump did not affect the cell volume change measurements. A constant axial load was applied to the top of the soil specimen using the Bellofram piston at the same time as the cell pressure was applied by opening the air pressure valve connected to the piston at the same time as applying the cell pressure. The change in cell volume and the change in height were monitored during this process using the cell volume burette on the pressure panel and the LVDT attached to the triaxial cell piston, respectively

Following assembly of the triaxial cell, the automated humidity control system was utilized to apply a specified value of total suction to the specimen by applying a target relative humidity to the bottom of the specimen. Time was permitted for suction equilibration, defined as the time required for the relative humidity at the top and bottom to reach the same value. The relative humidity and temperature at the bottom and top of the specimen during suction equilibrium is shown in Figure 5(a). Two hours were needed for the relative humidity at the bottom to reach the

target value, while an average of two weeks were needed for the relative humidity at the top to reach the same target value. After the target relative humidity at the top of the specimen was attained, at least six additional hours were allowed for uniformity of total suction throughout the soil specimen. This period of time is matched with Likos and Lu (2003) test results where they indicated that 2 to 5 hours were the time needed to reach constant water content and they allowed time from 9-12 hours to allow water content uniformity.

After this, the soil specimen was assumed to be in equilibrium under the externally applied stresses and internally applied suction when the axial deformations, recorded using the mounted LVDT, remained constant for at least 24 hours, as shown in Figure 5(b). After the soil specimen reaches equilibrium, the load frame was switched from load-control conditions to displacement control conditions. A constant displacement rate of 1.27×10^{-4} m/min was applied to shear the soil specimen. This rate was found to allow drained conditions during shearing (i.e., no change in relative humidity at the boundaries was noted). The unsaturated specimens evaluated in this study have degrees of saturation of less than 0.11, which is very close to the residual degree of saturation. It is not expected that there is sufficient water in the pores to become pressurized during the shearing process. Further, the relative humidity control system was operated during shearing to ensure that the suction remained constant during shearing. After shearing, the final water content of the soil specimen was measured and recorded. A summary of the results from the testing program are presented in Table 2.

Test Results

Consolidated undrained triaxial tests were performed on saturated specimens of Bonny silt at three different effective confining stresses in order to define the effective failure envelope. This failure envelope provides a baseline case to evaluate the results from high suction conditions,

and can also be used to define the critical state line. In addition, two sets of consolidated drained triaxial tests were performed on unsaturated specimens at suction values of 162 and 291 MPa (corresponding to degrees of saturation of 0.11 and 0.06, respectively) under net confining stresses of 100, 200, and 300 kPa. The void ratios of the specimens before shearing (i.e., after equilibration under the net confining stress and after application of high suction magnitudes for the unsaturated specimens, and after consolidation under the effective confining stress for the saturated specimens) are shown in Figure 6. The confining stress was applied to the unsaturated specimens before application of the target suction value. The results shown in Figure 6 indicate that the void ratio decreases with increasing suction and net confining stress, and a greater reduction in void ratio was observed when applying high suctions to specimens under an initially high net confining stress. It is possible that a difference in the equilibrium void ratio may have been different if high suction magnitudes were applied to the specimens before application of the net confining stress as the stiffness of the soil is expected to change significantly after application of high suction magnitudes.

The stress-strain curves for the saturated and unsaturated specimens are shown in Figures 7(a), 7(b), and 7(c) for the three different net confining stress values. The results in Figure 7 clearly indicate that the maximum principal stress difference and axial strain at failure increase as the suction value and the net confining stress increase. Further, a brittle failure mode was observed in the stress-strain curves for the specimens under high suction magnitudes, which differed significantly from the relatively smooth stress-strain curves of the saturated specimens. In Figure 7(c), the stress-strain curve corresponding to 162 MPa suction showed hardening at the beginning of the test due to the brief accidental application of a fast shearing rate to the specimen when checking the contact of the loading piston and specimen before the actual start of shearing

at the conventional rate. Although the stiffness from this test is not reliable, the results from this test still showed reasonable peak shear strength behavior. Due to the brittle failure mechanism noted in the unsaturated specimens, it was not possible to reach critical state conditions. Accordingly, only the peak shear strength values from the consolidated drained tests on the unsaturated specimens were used in the analysis.

The response of the pore-water pressure with respect to the axial strain during shearing of the saturated specimens is shown in Figure 8(a). The results in this figure indicate that the excess pore water pressures increase during shearing, and continue to increase after reaching the maximum principal stress difference. This means that the effective stresses is also continued decreasing during shearing and the compacted silt would tend to contract under drained conditions. The volumetric strain results for the unsaturated specimens sheared under drained conditions at a total suction of 291 MPa are shown in Figure 8(b), which show a clear dilation during shear. This difference in behavior between the saturated and unsaturated specimens is likely due to the reduction in void ratio during application of the high suction values, and also likely due to an increase in apparent preconsolidation stress with increasing suction. It can also be observed from Figure 8(b) that the amount of dilation decreases with confining stresses for the range of confining stresses evaluated in this study.

The drained failure envelopes for the saturated and unsaturated specimens sheared under room temperature are shown in Figure 9(a) in terms of net confining stress. The results show an increase in the shear strength of the soil with increasing suction and net confining stress. The fact that the unsaturated specimens still have an increase in shear strength with increasing confining stress indicates that they still behave as frictional materials (i.e., that application of high suction magnitudes did not cause them to behave like cemented materials). Because it is assumed that

unsaturated specimens have negligible excess pore water pressure generation during shearing, the failure envelopes from the CD triaxial tests represent drained failure envelopes even when plotted as a function of net normal stress. This trend is similar to the total suction failure envelopes reported by Nishimura and Fredlund (2000) for high suction magnitudes. The peak friction angle for the silt specimens at high suction magnitudes sheared under drained conditions ($\phi = 49°$) is larger than the effective friction angle defined from tests on saturated silt specimens ($\phi' = 29°$) corresponding to critical state conditions. The larger peak friction angle for the unsaturated specimens at high suction magnitudes may be due to an increase in preconsolidation stress and the shape of the steady-state boundary surface due to suction application, and to the large decrease in initial void ratio before shearing induced by application of the high suction magnitude. The void ratio at failure as a function of the maximum principal stress difference for both the saturated and unsaturated specimens at different suction values are shown in Figure 9(b). The results in this figure indicate that the shear strength increases with decreasing void ratio at failure, and that the results from saturated and unsaturated specimens follow the same nonlinear trend. The rate of increase in maximum principal stress difference decreases more substantially at very high suction values.

Analysis and Discussion

Evaluation of Linkages between the SSCC and SWRC

In order to evaluate the effective stress principle in unsaturated, compacted silt under low degrees of saturation, the SSCC calculated from the failure envelopes of the soil was compared with the SSCC obtained from the predictive approach involving the SWRC proposed by Lu et al. (2010). First, the slopes of the drained failure envelopes for the unsaturated specimens shown in Figure 8(a) were used to back-calculate two values of suction stress σ_s using Equation (5). A

third point on the SSCC was defined at the origin by virtue of the fact that the effective failure envelope for the saturated soil passes through the origin of the Mohr-Coulomb diagram.

The experimental SSCC is shown in Figure 10(a), along with the predicted SSCC obtained from Equation (5) with the fitting parameters α_{vG} and N_{vG} defined from the fitting of the van Genuchten (1980) SWRC model to the experimental SWRC in Figure 4(a). Although there are only two SSCC data points, the experimental SSCC indicates a nonlinear increase in suction stress with increasing suction. The predicted SSCC was found to over-predict the suction stress measured in the experiments by a significant amount. This behavior was attributed to the sensitivity of the suction stress to the value of N_{vG} observed in Figure 2(a). Specifically, small variations in the van Genuchten (1980) fitting parameters due to the experimental issues with the SWRC data shown in Figure 4(a) may have significant effects on the predicted SSCC. Accordingly, a second fitting of the van Genuchten (1980) SWRC model to the experimental SWRC data was performed in order to account for the error induced in the axis translation technique near the point where the water phase becomes discontinuous. The results of this fitting are shown in Figure 10(b) (dashed line), along with the original fitted SWRC (solid line). The new fitted SWRC still provides a reasonable fit to the experimental SWRC data, but in this case provides a much better prediction of the experimental SSCC data in Figure 10(a) (dashed line). This fitting exercise emphasizes the importance of careful and informed characterization of the SWRC when predicting the SSCC at high suction magnitudes from SWRC data obtained at lower suction ranges.

One of the possible reasons for the over-prediction of suction stress using the SWRC curve fitted to the data at low suctions might be the assumption that stresses arising from capillarity may still have major contribution to the suction stress in the pendular range of saturation. Also, it

is important to notice that application of high suctions using the vapor equilibrium technique has a major impact on the void ratio of the silt specimens evaluated in this study. The results in Figure 6 clearly show a large decrease in void ratio as the suction increase, which means that a SWRC defined using data from high and low suction values will not be for a constant void ratio. This means that predicting the SSCC from a SWRC with points having different void ratios can lead to inaccurate predictions in effective stress.

Evaluation of the Critical State Line for High Suction Magnitudes

The effective stress paths for the CU tests on saturated specimens and CD tests on unsaturated specimens are shown in Figure 11(a). The effective stress paths for the saturated specimens presented in this figure show behavior similar to normally consolidated soils where the effective stresses continue to decrease during shearing due to the increase in the pore-water pressure and specimens experienced a contraction for the specified range of normal stresses. The effective stress paths for the unsaturated specimens were calculated by plotting the measured values of principal stress difference versus the mean effective stress calculated using Equation (6) using the experimentally-fitted SSCC parameters from Figure 10(a) and the suction values back-calculated from the relative humidity measured at the bottom of the soil specimen during the shearing process. The effective stress paths for the unsaturated specimens shown in Figure 11(a) have a slope of 1:3, which is the same as the theoretical slope of the expected effective stress path in a drained triaxial test. This indicates that negligible excess pore water pressures were generated during shearing of the unsaturated specimens at low degrees of saturation. To better interpret the values of effective stress, the van Genuchten (1980) SWRC parameters fitted to the experimental suction stress data in Figure 10(a) were used to calculate the effective stress according to Equation (6). An evaluation of the critical state line (CSL) in

terms of mean effective stress is shown in Figure 11(b). Different from the Mohr-Coulomb failure envelopes shown in Figure 8(a), all of the shear strength values converge on a single peak shear strength failure envelope when the data is interpreted in terms of effective stress with slight shift to the left. It is clear that the peak shear strength failure envelope for the unsaturated specimens has a greater slope (M_{peak}) than that of the CSL defined from the shear strength tests on the saturated specimens (M_{CSL}). This is expected, as the application of high suctions to the specimens is expected to cause the specimens to behave like heavily overconsolidated soils, which by definition have a peak shear strength that is greater than the shear strength at critical state. Because the stress-strain curves for the specimens exhibited a brittle shape, it was not possible to characterize the critical state shear strength of the unsaturated specimens. Nonetheless, the fact that the shear strength of the unsaturated specimens tested at different net normal stresses and high suction magnitudes have peak shear strength values that converge on a single failure envelope reflects the validity of the effective stress principle at high suction magnitudes.

Another interesting observation from the results in Figure 11(b) is the fact that the specimens exhibit a clear linear relationship between peak shear strength and mean effective stress. This indicates that the effective stress definition of Skempton (1961) in Equation (2) is not necessary to describe the effective stress state in unsaturated silt under low degrees of saturation. In other words, the compressibility of the soil skeleton, which increased significantly during application of the high suction magnitudes, is likely still much greater than that of the soil particles. This conclusion may have been different if suction was applied to the specimens before application of the net normal stress value, which is a topic that deserves further study in the future.

Conclusion

The vapor flow technique developed by Likos and Lu (2003) for high suction application accompanied with the modified mechanical loading system into triaxial testing was successfully validated for the purpose of investigating the shear strength of compacted silts under low degrees of saturation. A substantial increase in peak shear strength was observed with total suction for the unsaturated soils under high suction magnitudes (a 40% increase over a change in suction of 129 MPa). The shear stress-strain curves show a more brittle failure mechanism than that measured for the same soil under saturated conditions, which prevents evaluation of critical state conditions for this specimens.

In addition, drained triaxial tests performed on unsaturated Bonny silt specimens under different combinations of total suction and net normal stress were used to evaluate the effective stress concept under low degrees of saturation. The SWRC model parameters obtained by fitting the SWRC to data from axis translation tests at low suctions were found to overestimate the suction stress by a significant amount. This was proposed to be due to the large change in void ratio observed during application of high suction magnitudes. An alternative fitting of the SWRC model was found to provide a better prediction of the SSCC while still providing a reasonable fit to the SWRC data at low suctions, reflecting the importance of careful characterization of the SWRC when predicting the SSCC at high suctions.

The use of the SSCC to define the effective stress for compacted silt under high suction magnitudes was found to reflect a consistent peak failure envelope in terms of mean effective stress plot shifted to a higher value of M at peak conditions ($M_{peak} = 1.98$). Although a clear peak failure envelope in terms of effective mean stress was observed, the brittle stress strain curves did not permit evaluation of effective stresses at critical state for unsaturated specimens under

high suction magnitudes. However, the value of M_{peak} was greater than the M value for critical state conditions ($M_{sat\text{-}CSL}$ = 1.23) defined using the consolidated undrained triaxial tests on saturated specimens. This behavior is consistent with that of heavily overconsolidated soils, which have a higher peak shear strength than the shear strength at critical state. This indicates that application of high suction magnitudes leads to a significant increase in preconsolidation stress in addition to the reduction in initial void ratio.

Acknowledgements

The first author would like to thank the Libyan government for financial support during her Ph.D. studies. The authors appreciate the support of the NSF grant CMMI-1054190. The views in this paper are those of the authors alone.

References

Ajdari, M., G. Habibagahi, H. Nowamooz, F. Masrouri, and A. Ghahramani. 2010. Shear strength behavior and soil water retention curve of a dual porosity silt-bentonite mixture. Scientia Iranica, pp. 430-440.

Alonso, E.E. and E. Romero. 2011. Experimental investigation on an effective stress law in compacted clayey/silty soil. Unsaturated Soils: Theory and Practice, pp. 331-336.

Alsherif, N. and J.S. McCartney. 2013. Triaxial cell for nonisothermal shear strength of compacted silt under high suction magnitudes. 1st PanAmerican conf. on Unsaturated Soils. Cartagena de los Indias, Colombia. 10 pg.

Bishop, A.W. 1959. The principle of effective stress. Teknisk Ukeblad I Samarbeide Med Teknikk, Oslo, Norway. 106(39), 859–863.

Bishop, A.W. and G.E. Blight. 1963. Some aspects of effective stress in saturated and partly saturated soils. Géotechnique 13, 177–197

Bishop, A.W. and I.B. Donald. 1961. The experimental study of partly saturated soil in triaxial apparatus. Proceedings of the 5th International Conference on Soil Mechanics and Foundation Engineering. Dunod, Paris. 13–21.

Blatz, J., J. Graham, and N. Chandler. 2002. Influence of suction on the strength and stiffness of high-plastic compacted clay. Canadian Geotechnical Journal. 39, 1005-1015

Blatz, A.J., Cui, Y.J., and Oldecop, L.A. 2008. Vapour equilibrium and osmotic technique for suction control. Geotechnical and Geological Engineering. doi:10.1007/s10706-008-9196-1

Blight, G.E. 1967. Effective stress evaluation for unsaturated soils. ASCE Journal of the Soil Mechanics and Foundations Division. 93(SM2), 125–148.

Brooks, R.H. and A.T. Corey. 1964. Hydraulic properties of porous media. Colorado State University Hydrology Papers No. 3, pp 1–27

Delage, P., E. Romero, and A. Tarantino 2008. Recent developments of controlling and measuring suction in unsaturated soils. Proceedings of the 1st European Conference on Unsaturated Soils, Durham, 33-52.

Escario, V. 1980. Suction controlled penetration and shear tests. Proceedings of the 4th International Conference on Expansive Soils. Vol II. Denver, CO. ASCE, pp. 781–797

Gallipoli, D., A. Gens, R. Sharma, and J. Vaunat. 2003. An elasto-plastic model for unsaturated soil incorporating the effects of suction and degree of saturation on mechanical behavior. Géotechnique. 53(1), 123–135.

Gray, W.G. and B.A. Schrefler. 2001. Thermodynamic approach to effective stress in partially saturated porous media. European Journal of Mechanics, A/Solids. 20(4), 521–538.

Hassanizadeh, S.M. and W.G. Gray. 1990. Mechanics and thermodynamics of multiphase flow in porous media including interphase boundaries. Advances in Water Resources. 13(4), 169–186.

Houlsby, G.T. 1997. Work input to an unsaturated granular material. Géotechnique 47(1), 193–196.

Kayadelen, C., M.A. Tekinsoy, and T. Taskıran. 2007. Influence of matric suction on shear strength behavior of a residual clayey soil. Environmental Geology. 53(4), 891-901.

Khalili, N., F. Geiser, and G. E. Blight. 2004. Effective stress in unsaturated soils: Review with new evidence. International Journal of Geomechics. 4(2), 115–126

Khalili, N. and M.H. Khabbaz. 1998. A unique relationship for χ for the determination of the shear strength of unsaturated soils. Géotechnique. 48(5), 681–687.

Khalili, N. and S. Zargarbashi. 2010. Influence of hydraulic hysteresis on effective stress in unsaturated soils. Géotechnique. 60(9), 729–734.

Khosravi, A., N. Alsherif, C. Lynch, and J.S. McCartney. 2012. Use of multistage triaxial testing to define effective stress relationships for unsaturated soils. ASTM Geotechnical Testing Journal. 35(1), 10pg.

Khosravi, A. and J.S. McCartney. 2012. Impact of hydraulic hysteresis on the small-strain shear modulus of unsaturated soils. ASCE Journal of Geotechnical and Geoenvironmental Engineering. 138(11), 1326–1333.

Likos, W.J. and N. Lu. 2001. Automated measurement of total suction characteristics in the high suction range: application to the assessment of swelling potential. Transportation Research Record. 1755, 119–128.

Likos, W.J. and N. Lu. 2003. Automated humidity system for measuring total suction characteristics of clay. Geotechnical Testing Journal, 26(2),

Loret, B. and N. Khalili. 2002. An effective stress elastic–plastic model for unsaturated porous media. Mechanics of Materials. 34(2), 97–116.

Lloret, A., M.V. Villar, M. Sanchez, A. Gens, X. Pintado, and E.E. Alonso. 2003. Mechanical behaviour of heavily compacted bentonite under high suction changes. Géotechnique 53(1), 27-40

Lu, N., J. Godt, and D. Wu. 2010. A closed-form equation for effective stress in unsaturated soil. Water Resources Research. 46, W05515.

Lu, N., and W.J. Likos. 2004. Unsaturated Soil Mechanics. Wiley, New York.

Lu, N. and W.J. Likos. 2006. Suction stress characteristic curve for unsaturated soil. Journal of Geotechnical Geoenvironmental Engineering. 132(2), 131–142.

McCartney, J.S. and D. Znidarcic. 2010. Test system for hydraulic properties of unsaturated nonwoven geotextiles. Geosynthetics International. 17(5), 355-363.

Ng, C.W.W., J. Xu and S.Y. Yung. 2009. Effects of imbibition-drainage and stress ratio on anisotropic stiffness of an unsaturated soil at very small strains. Canadian Geotechnical Journal. 46(9), 1062-1076.

Nishimura, T. and D.G. Fredlund. 2000. Relationship between shear strength and matric suction in an unsaturated silty soil. UNSAT ASIA 2000, Singapore, May 18-19, 563-568

Nuth, M. and L. Laloui. 2008. Effective stress concept in unsaturated soils: Clarification and validation of a unified framework. International Journal for Numerical and Analytical Methods in Geomechanics. 32, 771–801.

Oberg A. and G. Sallfors. 1997. Determination of shear strength parameters of unsaturated silts and sands based on the water retention curve. Geotechnical Testing Journal. 20(1), 40–48.

Sheng D., D.G., Fredlund, and A. Gens. 2008. A new modelling approach for unsaturated soils using independent stress variables. Canadian Geotechnical Journal. 45, 511–534.

Skempton, A.W. 1961. Effective stress in soils, concrete, and rocks. Pore Pressure and Suction in Soils, Butterworths, London, pp. 4–16.

Tamagnini, R. 2004. An extended cam-clay model for unsaturated soils with hydraulic hysteresis. Géotechnique. 54(3), 223–228.

Toll D.G. and B.H. Ong. 2003) Critical state parameters for an unsaturated residual sandy clay. Géotechnique 53(1), 93–103.

Vanapalli, S.K., D.G. Fredlund, and D.E. Pufahl. 1996. The relationship between the soil-water characteristic curve and the shear strength of a compacted glacial till. ASTM Geotechnical Testing Journal. Vol. 19(3), 259–268.

van Genuchten, M.T. 1980. A closed-form equation for predicting the hydraulic conductivity of unsaturated soils. Soil Science Society of America Journal. 44, 892–898.

Wheeler, S.J., R.S. Sharma, and M.S.R. Buisson. 2003. Coupling of hydraulic hysteresis and stress–strain behaviour in unsaturated soils. Géotechnique, 53(1), 41–54.

List of Tables and Figures

the saturated specimens; (b) Volume change as a function of axial strain for the unsaturated specimens at a suction of 291 MPa

Fig. 9. Results from triaxial tests on saturated and unsaturated silt specimens at a constant temperature of 23 °C: (a) Effective and total stress failure envelopes for saturated specimens and effective stress failure envelopes for unsaturated specimens (not to scale); (b) Void ratio at failure versus principal stress difference for different suction magnitudes

Fig. 10. SWRCs and SSCCs fitted to the experimental data (different values of α_{vG} and N_{vG}): (a) SSCCs; (b) SWRCs

Fig. 11. Critical state analysis for Bonny silt at different suction values obtained using the experimental SSCC parameters: (a) Effective stress paths obtained using suction stress values calculated from the suction applied to bottom of the specimen; (b) Mean effective stress plot with mean effective stress obtained using the experimental SSCC

Table 1. Geotechnical index properties of Bonny silt

Parameter	Value
Liquid limit, LL	25
Plastic limit, PL	21
Specific gravity, G_s	2.65
Standard Proctor optimum gravimetric water content, w_{opt}	13.6%
Standard Proctor optimum gravimetric dry density, $\gamma_{d,max}$	16.3 kN/m^3

Table 2. Summary of results from consolidated-drained triaxial tests on unsaturated specimens

Suction	Net normal stress	Relative humidity at equilibrium	Final water content	Initial void ratio	Void ratio at suction equilibration	Principal stress difference at failure	Mean effective stress at failure
ψ (kPa)	p_{net} (kPa)	R_h (%)	w_f	e_i	e_s	$(\sigma_1-\sigma_3)_f$ (kPa)	$(\sigma'_1-2\sigma'_3)_f/3$ (kPa)
162000	100	30.5	2.1	0.682	0.57	1887	1053
162000	200	30.6	2.2	0.680	0.50	2477	1383
162000	300	29.8	2.3	0.682	0.51	3101	1724
291000	100	12.0	0.8	0.689	0.48	2306	1278
291000	200	11.8	1.6	0.663	0.49	2986	1638
291000	300	12.0	0.4	0.684	0.39	3273	1867

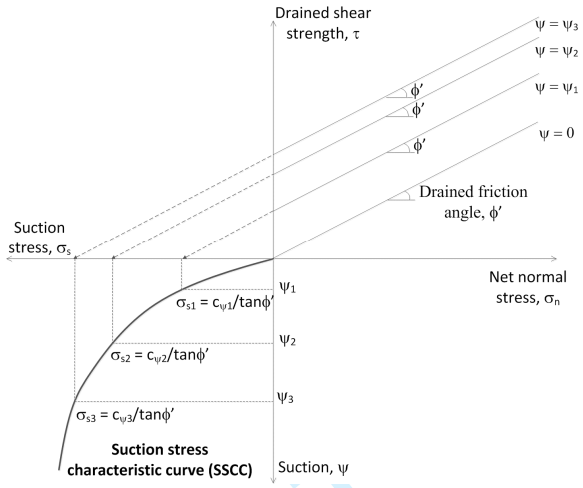

Fig. 1. Schematic showing the definition of the suction stress vs. matric suction relationship using drained failure envelopes (after Lu and Likos 2006)

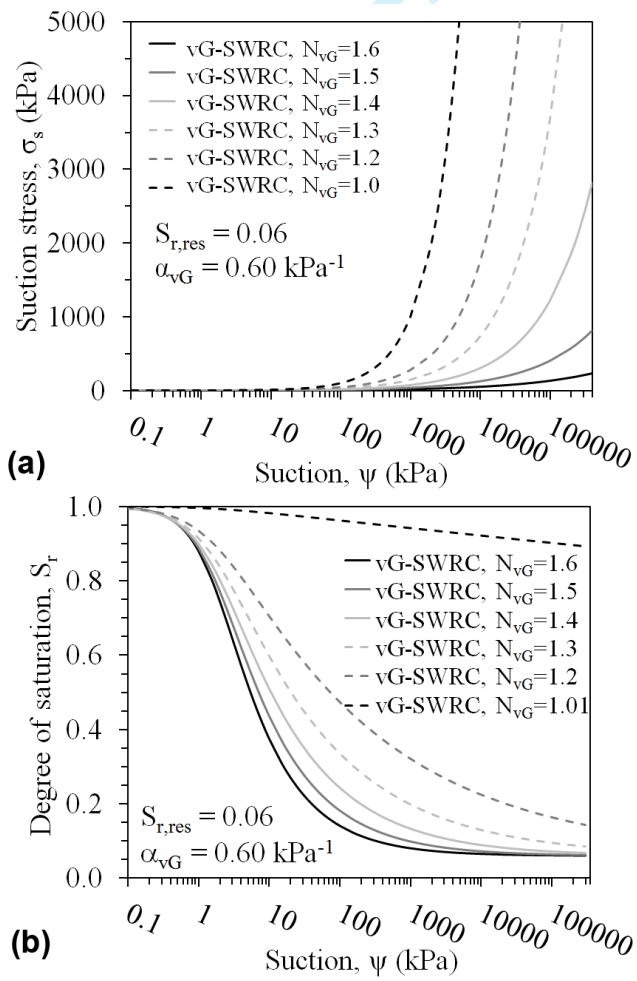

Fig. 2. Impact of N_{vG} on the shapes of the SWRC and SSCC (constant value of $\alpha_{vG} = 0.60$ kPa^{-1}): (a) SSCC; (b) SWRC

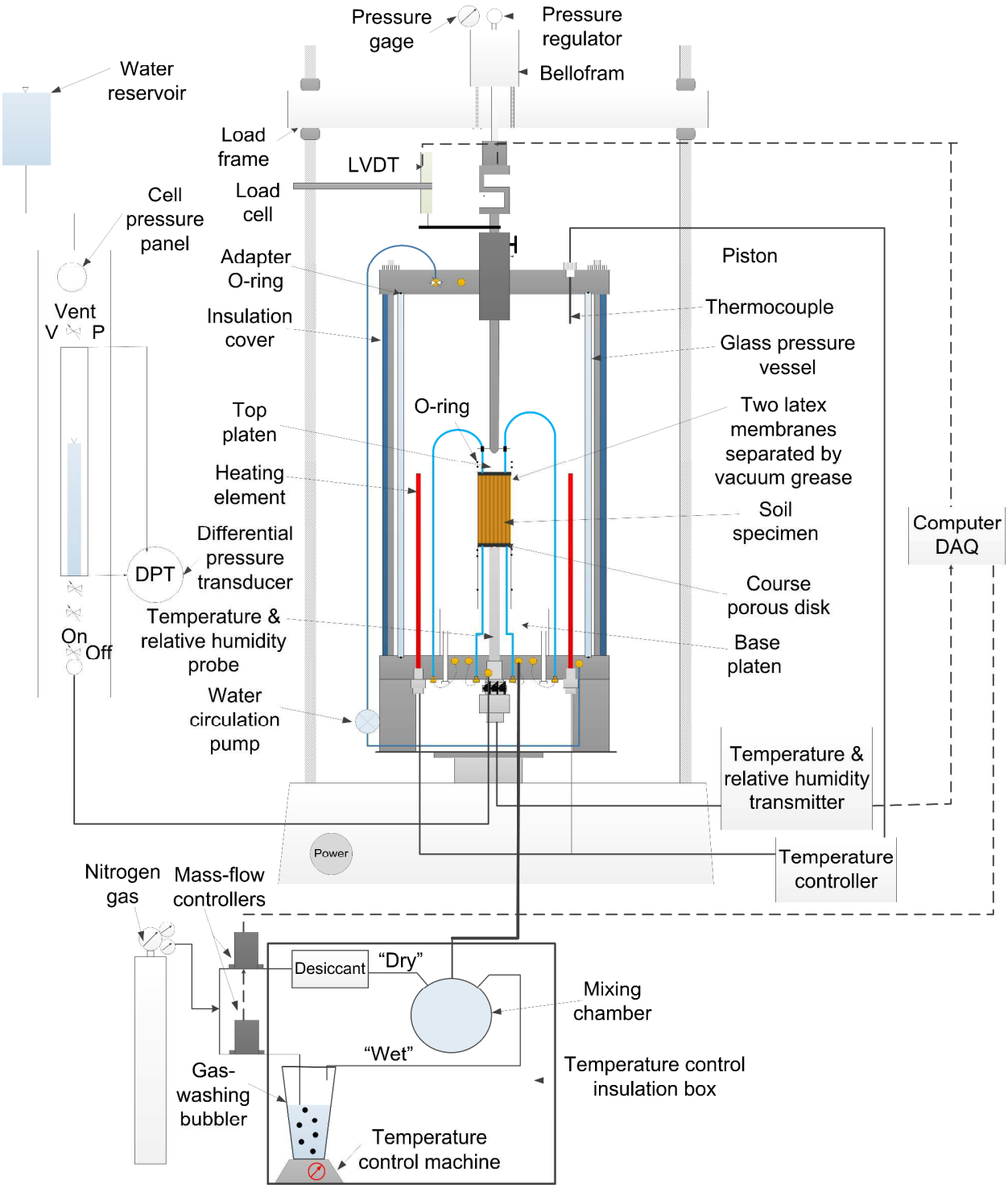

Fig. 3. Schematic of thermo-hydro-mechanical triaxial setup for testing soils under high suction magnitudes (the temperature control capability is used in this test program to maintain constant room temperature)

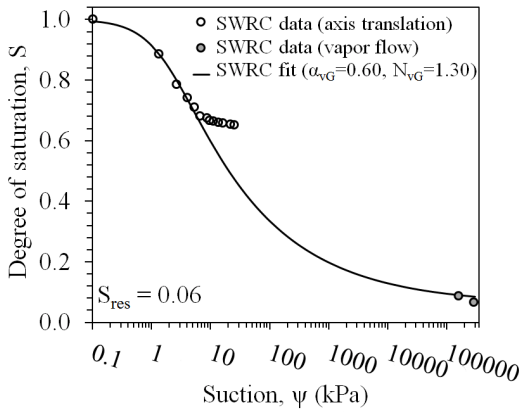

Fig. 4. SWRC for compacted Bonny silt obtained by fitting data to the results from the axis translation technique

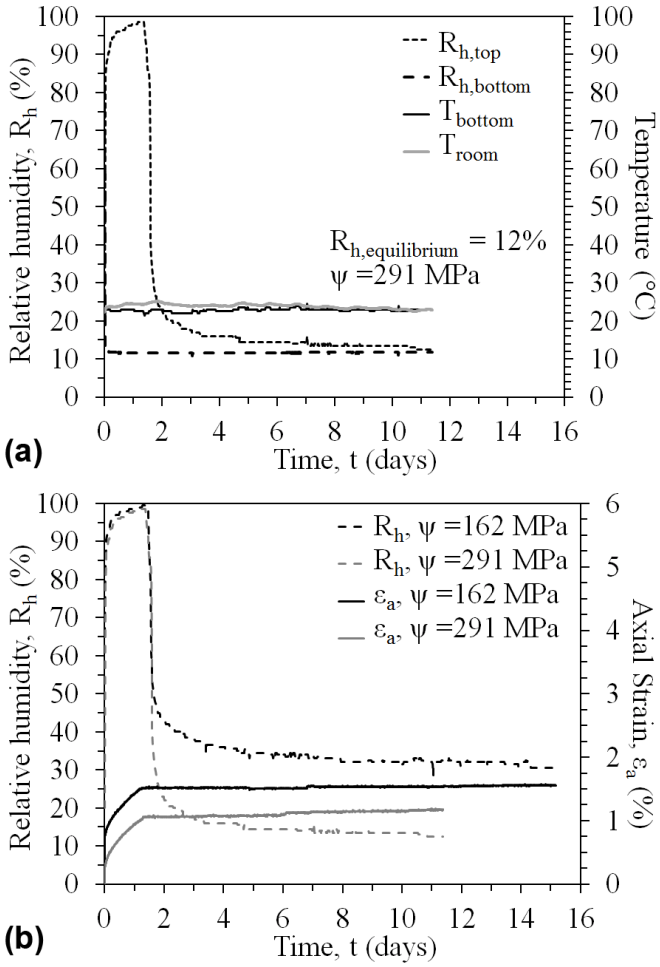

Fig. 5. Equilibration processes for tests performed at a net confining stress of 100 kPa: (a) Relative humidity recorded at the top and bottom of a soil specimen along with the specimen and room temperatures; (b) Relative humidity at the top of the specimen and axial strain for specimens at different suction values

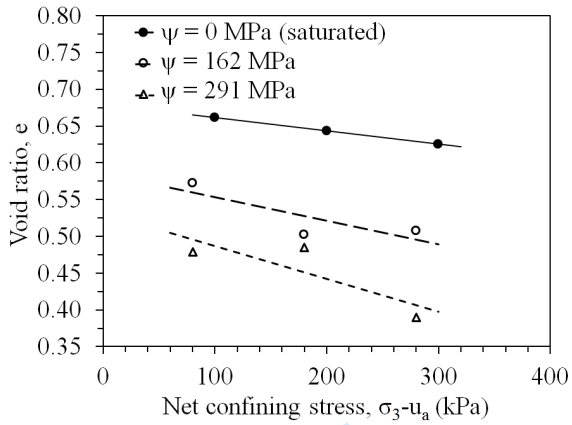

Fig. 6. Initial void ratios of the silt specimens before shearing under different net confining stress values (i.e., after consolidation and/or equilibrium under the applied suction)

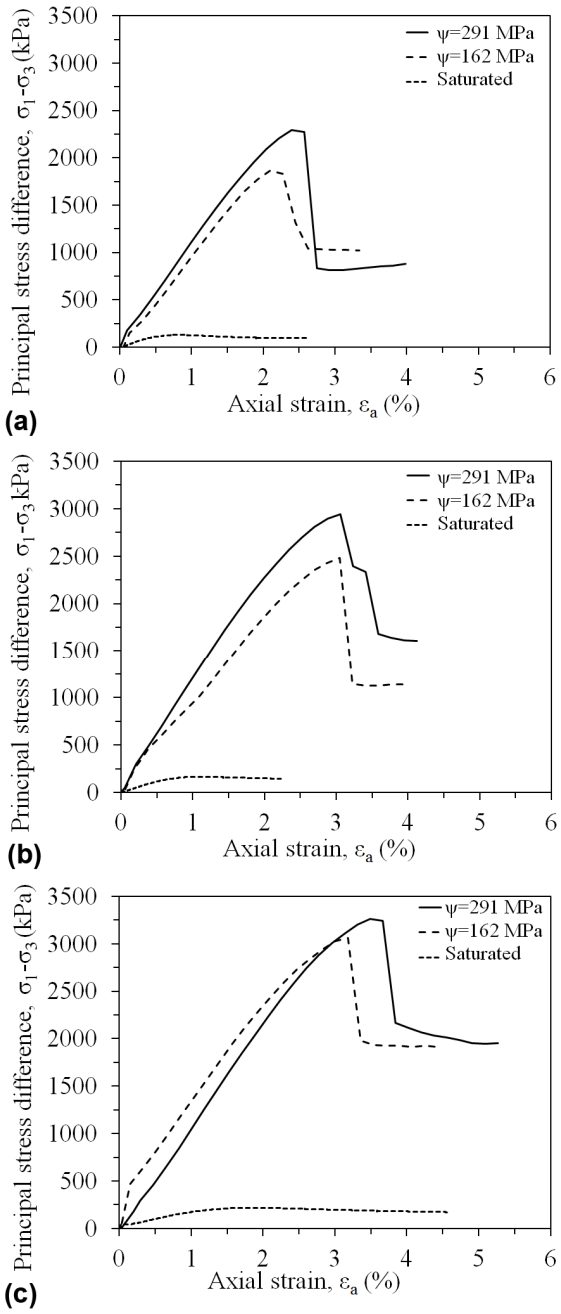

Fig. 7. Stress-strain curves for saturated and unsaturated Bonny silt specimens under at net confining stresses of: (a) 100 kPa; (b) 200 kPa; (c) 300 kPa

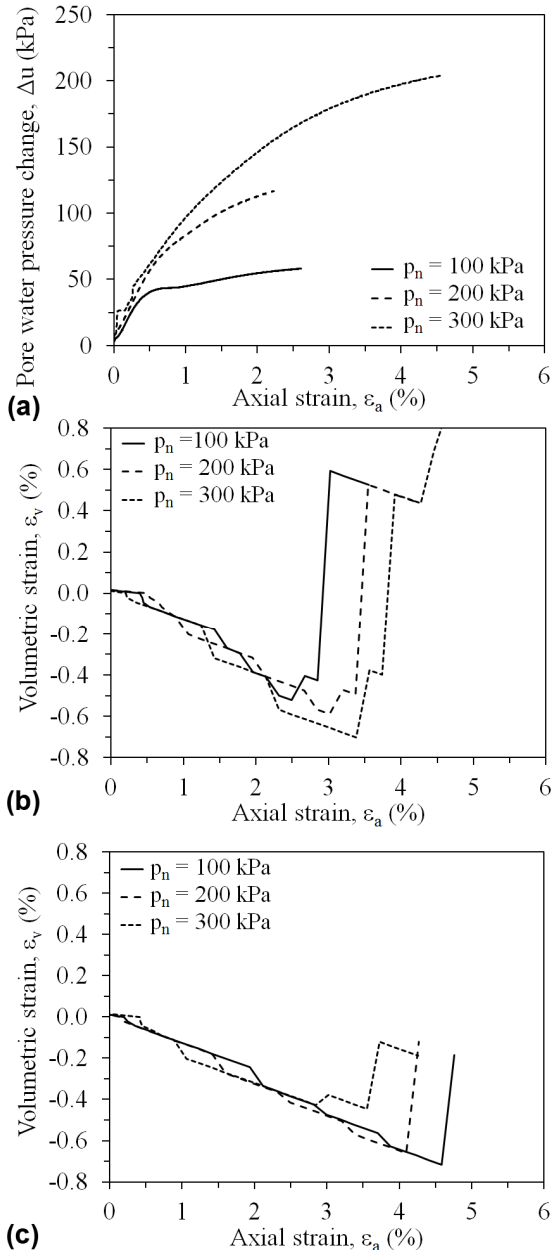

Fig. 8. Results from triaxial tests on saturated and unsaturated silt specimens at various net confining stresses: (a) Excess pore water pressure generation as a function of strain for the saturated specimens; (b) Volume change as a function of axial strain for the unsaturated specimens at a suction of 162 MPa; (c) Volume change as a function of axial strain for the unsaturated specimens at a suction of 291 MPa

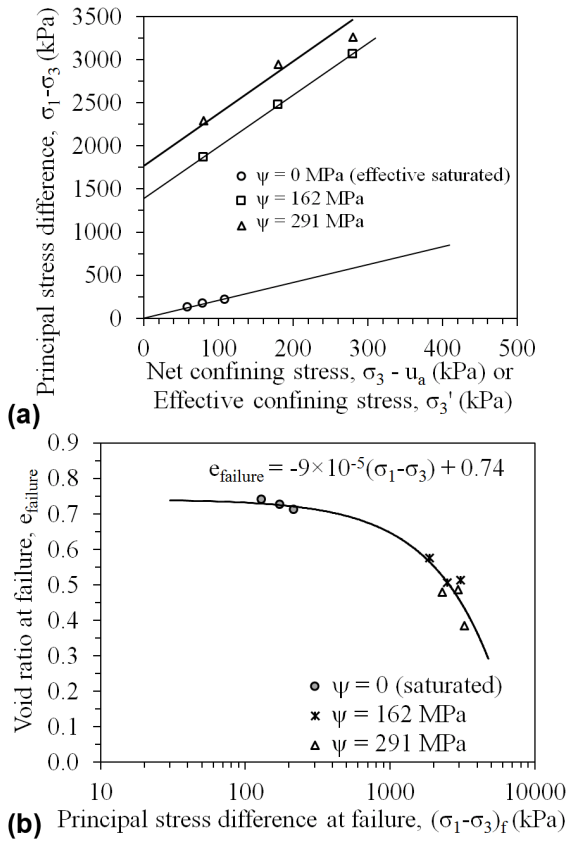

Fig. 9. Results from triaxial tests on saturated and unsaturated silt specimens at a constant temperature of 23 °C: (a) Effective and total stress failure envelopes for saturated specimens and effective stress failure envelopes for unsaturated specimens (not to scale); (b) Void ratio at failure versus principal stress difference for different suction magnitudes

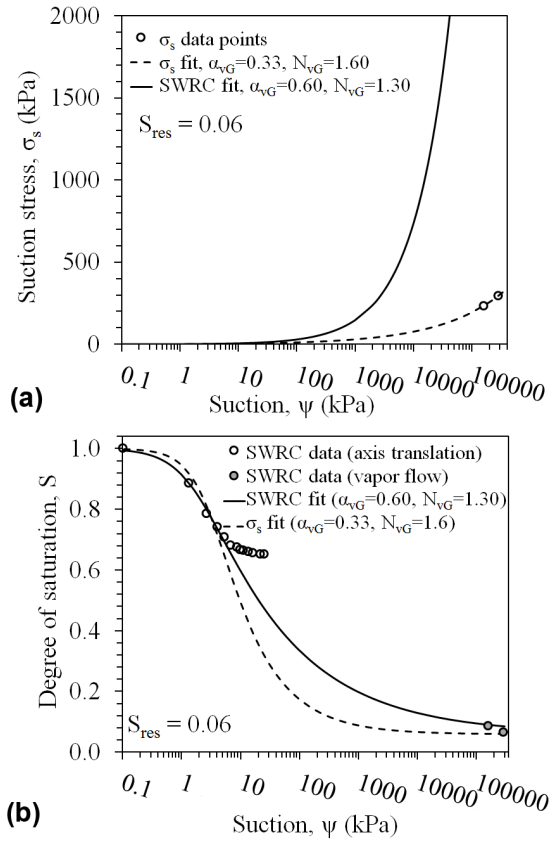

Fig. 10. SWRCs and SSCCs fitted to the experimental data (different values of α_{vG} and N_{vG}): (a) SSCCs; (b) SWRCs

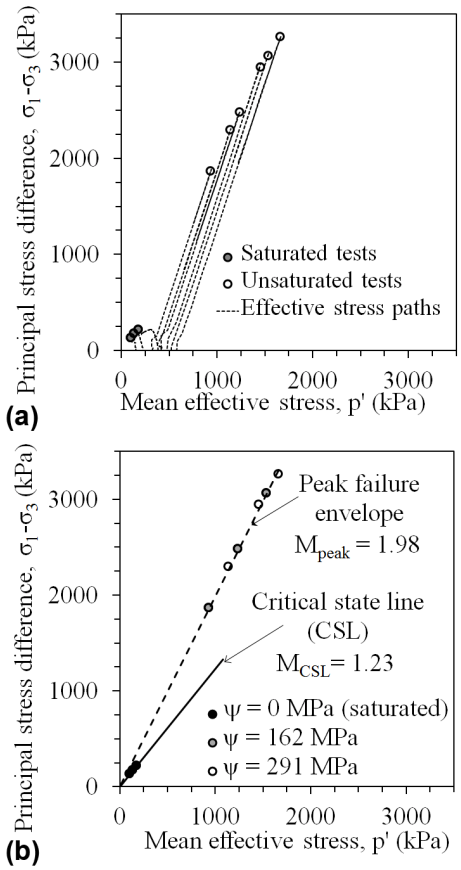

Fig. 11. Critical state analysis for Bonny silt at different suction values obtained using the experimental SSCC parameters: (a) Effective stress paths obtained using suction stress values calculated from the suction applied to bottom of the specimen; (b) Mean effective stress plot with mean effective stress obtained using the experimental SSCC